Ocean stratification and sea-ice cover in Barents and Kara seas modulate sea-air methane flux: satellite evidence

L. Yurganov[1], D. Carroll[2] , and H. Zhang[3]

[1]University of Maryland Baltimore County, Baltimore, Maryland, USA

[2] Moss Landing Marine Laboratories, San José State University, CA, USA

[3]Jet Propulsion Laboratory, California Institute of Technology, CA, USA

Corresponding author: Leonid Yurganov (Leonid.Yurganov@gmail.com)

Key Points:

- Positive methane anomalies over the Barents and Kara Seas in winter coincide with increasing mixed layer depth.
- Seventeen years of satellite AIRS data reveal areas of enhanced rates of methane growth in the northern Barents/Kara Arctic region.
- The methane seasonal cycle amplitude grows from 2002 to 2019 most rapidly over areas with maximal rates of sea-ice degradation.

INDEX TERMS

0312 Air/sea constituent fluxes

1615 Biogeochemical cycles, processes, and modeling

1640 Remote sensing

3002 Continental shelf and slope processes

3004 Gas and hydrate systems

Abstract

The diverse range of mechanisms driving the Arctic amplification are not completely understood and, moreover, the role of the greenhouse gas methane in Arctic warming remains unclear. Strong sources of methane at the ocean seabed in the Barents Sea and other polar regions are well documented. Nevertheless, those data suggest that negligible amounts of methane fluxed from the seabed enter the atmosphere, with roughly 90% of the methane consumed by bacteria. The observations are taken during summer, which is favorable for collecting data but also characterized by a strongly-stratified water column. In winter the stratification weakens and after a breakdown of the pycnocline, convection, storms, and turbulent diffusion can mix the full-depth water column in high latitudes. The Mixed Layer Depth (MLD) in the ice-free Central/Southern Barents Sea is deepening and the ocean-atmosphere methane exchange increases. An additional barrier for the air-sea flux is seasonally and interannually variable sea-ice cover in partially ice-covered seas. We present Thermal IR space-based spectrometer data between 2002 and 2019 that shows increased methane concentration anomalies over the Barents and Kara seas in winter months. The seasonal methane cycle amplitude north of the Kara Sea has more than doubled since the beginning of the century; this may be interpreted as an effect of sea-ice decline and/or an evidence for growth of seabed emissions. A progressing degradation of Arctic sea-ice cover may lead to increased methane flux and, through a positive feedback loop, to further warming.

Plain Language Summary

Long-term satellite measurements of methane over the Arctic Ocean evidence that vertical seawater mixing is a significant factor that affects its concentration in the troposphere in winter. The methane seasonal amplitude over the northern Kara Sea has increased since the beginning of this century and a decline of the sea ice may be a reason for that.

1 Introduction

The Arctic has experienced the fastest warming on Earth over recent decades, with the Arctic Ocean warming at nearly double the rate of the global ocean (Hoegh-Guldberg and Bruno, 2010). The area, thickness, and concentration of sea-ice cover, has been significantly reduced (Comiso et al., 2008; Årthun et al., 2019). There is concern about the release of large amounts of the climate-active greenhouse gas methane (CH_4) from hydrates, permafrost, and other seabed reservoirs (James et al., 2016). The radiation warming potential of methane is 28–34 times that of carbon dioxide (CO_2) over a 100-year period (Myhre et al., 2013). The Barents and Kara seas (BKS) have extensive reserves of oil and natural gas (Shipilov and Murzin, 2002). Thermogenic (fossil) methane seeps through faults in sedimentary layers in the BKS. For example, Serov et al. (2017) reported on intensive cold seep activity clustered on the tops of several ~500-m-wide domes at depths of 370–390 m in Storfjordrenna, northwestern Barents Sea. A review article (James et al., 2016) describes the principal processes that regulate methane distribution in Arctic seafloor sediments, modification in the water column, and subsequent release to the atmosphere. Enhanced concentrations of dissolved methane in the Arctic Ocean seawater are widely observed; these are related, in part, to direct seeps of thermogenic methane, dissociation of gas hydrates and thawing of submerged permafrost. Methane is slowly oxidized by methanotrophic bacteria in oceanic deep layers below the pycnocline with timescales of weeks or years (James et al., 2016). As noted by James et al. (2016), the effect of reduced sea-ice cover on ocean-to-atmosphere methane emissions are especially poorly constrained. The satellite data presented here allow one to fill this critical gap. Warm Atlantic currents make the BKS a climatically important region (Skagseth et al. , 2020). A decline in BKS sea-ice in early winter influences

synoptic processes across the northern hemisphere (Petoukhov and Semenov, 2010; Årthun et al., 2019). The Barents Sea is a shallow sea (average depth 230 m), with depressions up to 400 m. The Kara Sea is even shallower (average depth 100 m). The release of methane from the seabed as a result of degradation of the submarine permafrost (Portnov et al., 2014) is expected in the Kara and southern Barents Seas. The most of Barents Sea is free of sea-ice year-round, while winter sea-ice cover in the Kara Sea, as well as in the northernmost Barents Sea, underwent a dramatic decline since early 2000s (Zhang et al., 2018b).

The presence of sources is just one necessary condition for methane to enter the atmosphere; transport of the gas from the seafloor to the ocean surface is also critically important. According to Rudels (1993), the relatively warm and salty layer of Atlantic Water (AW) provides a stratified barrier that can inhibit the penetration of dissolved gases into the ocean-surface layer during summer/early autumn (between June and October). Numerous direct studies have shown that during this season the flux in the Barents-Svalbard area is negligible (Gentz et al., 2014; Myhre et al., 2016; Mau et al., 2017). These field investigations, however, also identified strong sources at the seafloor and large concentrations of dissolved methane in deep ocean waters. Therefore, the flux of methane may be significant only after a breakdown of the pycnocline in November, and subsequent deepening of the MLD. The MLD increases sharply in November, with the bulk of the Barents Sea water column mixed by December (Kara et al., 2002). Increased turbulent diffusion is expected to facilitate methane fluxes to the atmosphere.

Methane over the BKS was measured from space by IASI (Infrared Atmospheric Sounding Interferometer) and AIRS (Atmospheric InfraRed Sounder) sounders (Yurganov et al, 2016, 2017, and 2019). Preliminarily, Yurganov et al. (2016) assessed the annual Arctic Ocean CH_4 emissions in 2010-2014 as ~ 2/3 of land CH_4 emission for north of 60° N. Saunois et al. (2020) estimated the latter as 23 ± 1 Tg CH_4 per year. So, the Arctic marine emission may be as large as 15 Tg CH_4 per year. Satellite observations in the Thermal IR (TIR) range are extremely useful for characterizing methane over ocean regions, particularly during the polar night. Other observational approaches, such as space-borne Short-Wave IR sensors (e.g., TROPOMI, the TROPOspheric Monitoring Instrument) require sunlight and cannot make observations during the polar night (Supplement Figure S1). Additionally, ship-based observations are logistically challenging in these ice-choked regions. Here we analyze methane concentrations in the lowest tropospheric layer over BKS estimated from AIRS/Aqua, IASI-1/MetOp-A with a focus on the November–January period. Data from the Cross-Track Infrared Sounder (CrIS) deployed at the Suomi National Polar-orbiting Partnership (SNPP) platform for 2015–2019 (Bloom, 2001)) were used as well. These data are coupled with regular satellite microwave measurements of sea-ice concentration, described by Cavalieri et al. (1996). MLD was computed from the "Estimating the Circulation and Climate of the Ocean" (ECCO) consortium (Wunsch et al., 2009) ocean state estimate. We find that both vertical mixing and sea-ice cover significantly impacted methane concentrations. Our results provide a basis for predicting the growth of future Arctic Ocean methane emissions, in assumption that sea-ice cover continues to decline.

2 Methods

2.1 Satellite instruments, methane data, and retrieval techniques

AIRS, IASI, anf CrIS belong to the TIR group of hyper-spectral sounders (their characteristics are listed by Smith and Barnet (2019)). An important advantage of them is a capability to work at night and over water surface. A disadvantage is a reduced sensitivity to lower troposphere (Yurganov et al., 2016).

The AIRS diffraction grating spectrometer was launched in a sun-synchronous polar orbit

in May 2002 on board the Aqua satellite (Xiong et al., 2008). The instrument scans ± 48.3° from the nadir, which provides full daily coverage in the Arctic. Spectral resolution is 1.5 cm^{-1} at the methane ν4 absorption band near 7.65 μm. Currently (August 2020), the AIRS is still operational. Starting in September 2002, methane data were processed consistently using version 6 of the standard algorithm developed by NASA (Susskind et al., 2014). Monthly average Level 3 methane, surface and air temperatures between October 2002 and January 2020, both ascending and descending orbits, are available on-line on a 1°x1° latitude/longitude grid (AIRS3STM.006): https://disc.gsfc.nasa.gov/datasets/. Methane profiles were obtained for a 3×3 matrix of 9 pixels with a diameter of 13.5 km in nadir each.

The IASI-1/MetOp-A is a cross-track-scanning Michelson interferometer that measures spectra of outgoing long wave radiation with an apodized resolution of 0.5 cm−1 in the TIR spectral range that includes the ν4 CH_4 band near 7.65 μm wavelength (Razavi et al., 2009). The MetOp-A satellite, operated by EUMETSAT, was launched in 2006. Like AIRS, IASI has a 2200-km swath with a scan swath angle of ±48.3°. The IASI retrieval algorithm NUCAPS was built at NOAA/NESDIS to emulate the AIRS Version 5 code and has been in operation since 2008 (Maddy et al., 2009; Gambacorta, 2013). Level 2 data for 2×2 matrices of 4 circular, 12-km diameter pixels are available from the NOAA's CLASS site https://www.avl.class.noaa.gov/saa/products/search?sub_id=0&datatype_family=IASI&submit.x=27&submit.y=10.

The CrIS is a Michelson interferometer deployed at the SuomiNPP platform launched in October, 2011, in a sun-synchronous polar orbit. Apodized full spectral resolution is 0.75 cm^{-1}. Methane profiles were obtained for a 3×3 matrix of 9 pixels with a diameter of 14 km in nadir each. Retrieval technique CLIMCAPS was developed in Science and Technology Corporation, Columbia, MD, and funded by NASA (Smith and Barnet, 2019). The Level 2 data coded as SNDRSNIML2CCPRET are available from the Goddard Earth Sciences Data and Information Services Center (GES DISC), https://disc.gsfc.nasa.gov/datasets/SNDRSNIML2CCPCCR_2/summary.

The Thermal IR reliable measurements require the surface to be warmer than air above it. The data were filtered for cases of Thermal Contrast ThC> 10° C (Yurganov et al., 2016 and Supplement Figures S2 and S3) , where $ThC = T_{surf}-T_{600}$, T_{surf} is surface temperature, and T_{600} is air temperature at 600 hPa air pressure . Figure S4 in the Supplement illustrates influence of filtering for AIRS data.

The profiles were averaged for the lower troposphere (LT) from the surface to the level of 600 hPa (~ 4 km) and from 600 hPa to 400 hPa (mid troposphere, MT). The sensitivity to methane variations in the LT and MT was estimated empirically by comparison with simultaneous aircraft measurements at three stations in the United States (Yurganov et al., 2019, and Supplement Figure S4). LT sensitivity was found in the range of 0.3-0.5. MT sensitivity was estimated as 0.8-1.2, i.e., significantly higher. A physical meaning of the empirical sensitivity is a change in retrieved concentration that corresponds to the unit change of the "true" value. E.g., the sensitivity 0.5 means that real variations (not concentrations themselves) are underestimated by 100%. For the first glance, preference should be made to mid tropospheric data. However, variations of mid tropospheric data are critically dependent on air transport. So, we have chosen to focus on the LT data in attempt to get information on methane as close as possible to the surface. Data for MT are placed in the Supplement (Figures S5, S6, and S7).

2.2 ECCO Estimates of Mixed Layer Depth

To compute MLD, we use the ECCO LLC270 global ocean and sea-ice data synthesis (Zhang et al., 2018a). ECCO LLC270 is built upon two previous ECCO efforts, ECCO v4 (Forget et al., 2015) and ECCO2 (Menemenlis et al., 2005a, 2005b, 2008; Fenty et al., 2017). Compared to the lower-resolution ECCO v4 synthesis (nominal 1° grid spacing), ECCO LLC270

has finer horizontal grid spacing (~1/3° at the equator and ~18 km at high latitudes). The vertical discretization comprises 50 z-levels; model integration spans January 1992 to December 2018. Terrestrial runoff along coastal boundaries is forced using the monthly climatology of Fekete et al. (2002). Since horizontal resolution is insufficient to resolve mesoscale eddies, their impact on the large-scale ocean circulation is parameterized using the Redi (1982) and Gent and McWilliams (1990) schemes.

We compute monthly-mean LLC 270 MLD using three criteria: (1) when the potential density is greater than surface-ocean density x 0.125 kg m^{-3} (Suga et al., 2004); (2) when the potential density is larger than surface-ocean density ρ by 0.8°C x α, where ρ is the density and α is the seawater thermal expansion coefficient at the ocean surface (Kara et al., 2000); and (3) when the potential density is greater than surface-ocean density + 0.03 kg m^{-3} (Boyer et al., 2004). Kara et al. (2002) compared calculations by criterion #2 with field measurements and confirmed that method accuracy is better than 20 m.

2.3 Satellite Sea-ice Observations

Sea-ice concentration data are archived by the NASA National Snow and Ice Data Center Distributed Active Archive Center (https://nsidc.org/data/NSIDC-0081/versions/1; described by Cavalieri et al., 1996). The mean monthly data set for November, 2003–January, 2020 is generated from the surface brightness temperature data and is designed to provide a consistent time series of sea-ice concentration C_{ice} (the fraction of ice for each 20 × 20 km^2 pixel) spanning the coverage of two passive microwave instruments developed as a part of the Defense Meteorological Satellite Program (DMSP), DMSP-F8 and Special Sensor Microwave Imager/Sounder (SSMIS) DMSP-F17. In this paper, we use also the fraction of open water: $C_{wat} = 1 - C_{ice}$ for comparison with concentration and seasonal cycles of methane.

3 Results

Maps of monthly mean LT Arctic methane concentrations for 2013, retrieved from the IASI-1 orbital measurements, have been published by Yurganov et al., (2016) and for 2018 by Yurganov et al. (2019). Here we present seasonal maps for the period between February, 2019 and January, 2020, retrieved from AIRS data. All data were binned into 3-month seasons, conditionally named "spring" (Feb–Apr.), "summer" (May–Jul), "autumn" (Aug–Oct.), and "winter" (Nov–Jan) (Figure 1). The summer methane distribution over the Arctic (Figure 1b) is essentially flat, but in autumn–winter (Figure 1c and 1d) peculiar positive anomalies were observed over BKS and other seas. Similar anomalies. but less contrast, were observed for MT altitudes between 4 and 6 km (Supplement, Figure S5). To study this phenomenon, three domains were selected (Figure 1). Domain #1 is free of sea-ice in winter, and is located in the relatively deep western Barents Sea (mean depth 379 m). Domain # 2 is located between three archipelagos: Franz-Joseph Land (FJL), Severnaya Zemlya (SZ) and Novaya Zemplya (NZ). It is shallower (mean depth 82 m) and partially covered by sea-ice. A control domain #3 with mean depth 2053 m was selected in the Norwegian Sea.

Monthly mean concentrations for domains # 1 and # 3, retrieved from data of three space-borne spectrometers covering 2010–2018, were computed. Figure 2 shows the general agreement between excess methane in domain #1 (differences between domains 1 and 3) delivered by three independently operating instruments: IASI, AIRS, and CrIS. All three demonstrate a maximum in December–January and minimum in June–August.

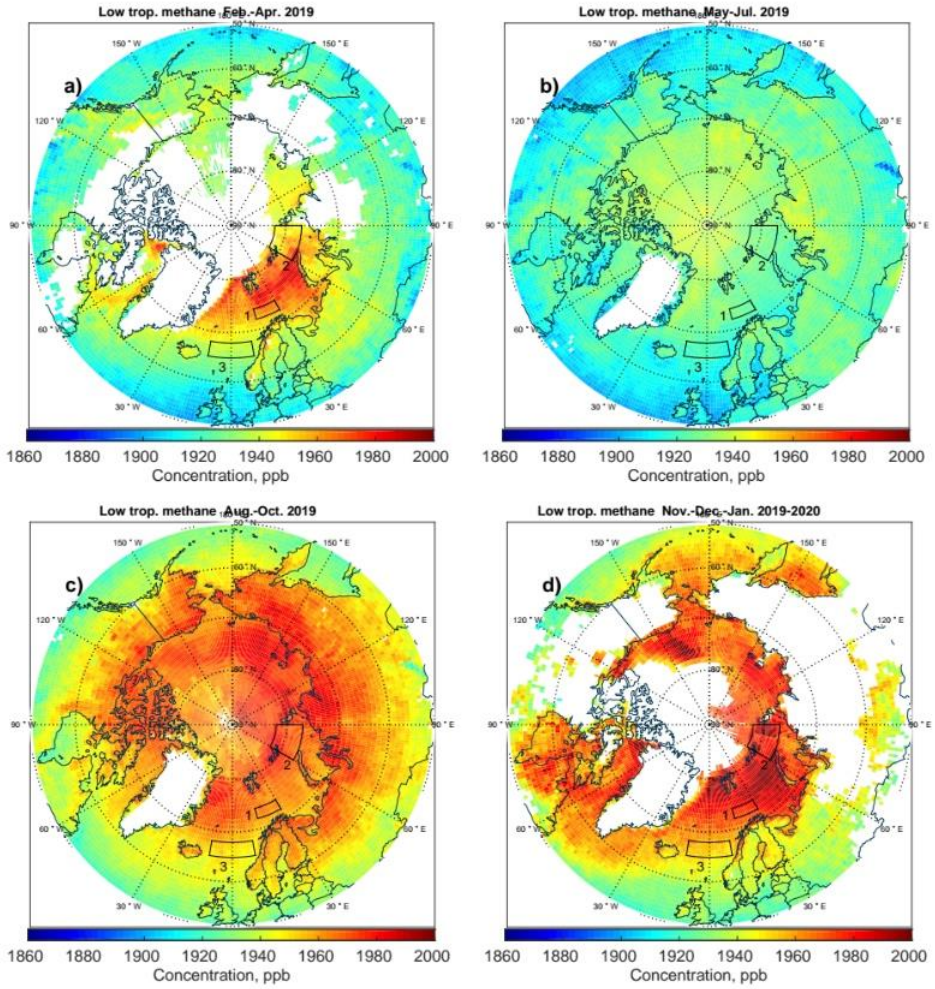

204 *Figure 1*

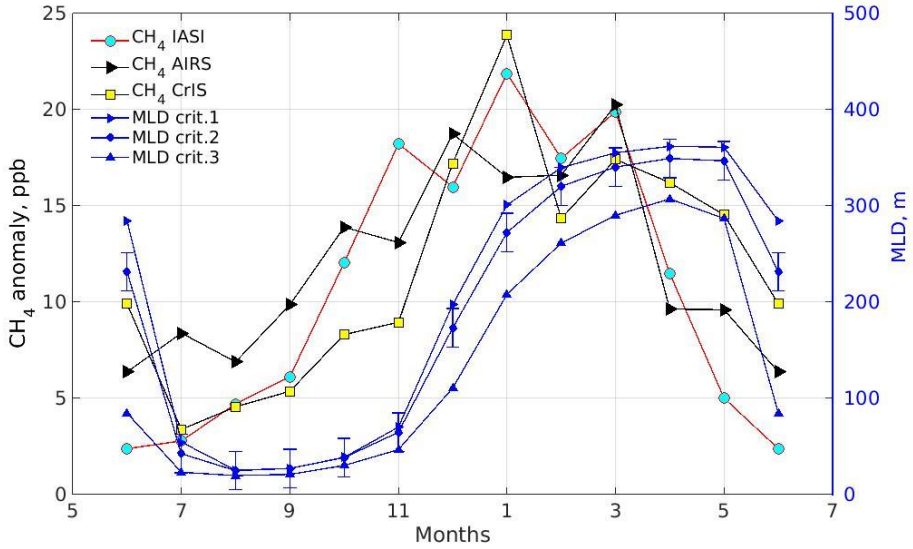

205 *Figure 2*

206 To explain this pattern, we computed MLD in domain #1 over the same time period using
207 three different criteria (see Methods). These MLD estimates have similar shapes, but somewhat

different magnitudes, which might be taken as an estimate of data accuracy. Kara et al. (2002) estimated accuracy as ± 20 m for the data based on criterion #2. Only in June do the plots diverge, otherwise disagreements do not exceed 50 m. Methane anomaly steeply grows in October–November and reaches a maximum in January. MLD is very shallow in summer (~20-30 m), abruptly grows between November and December, and plateaus by February.

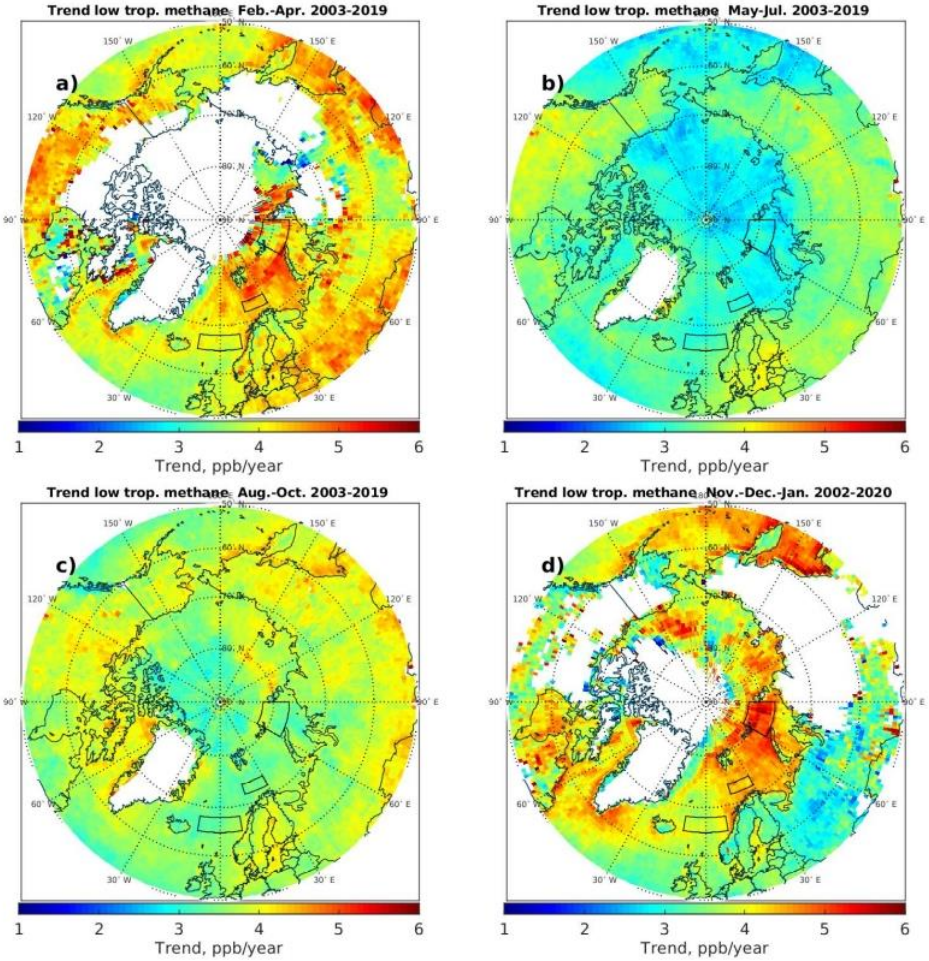

Figure 3

A strengthening of winter anomalies throughout the seven-years-long period between 2010 and 2016 have been noted by Yurganov et al. (2017). A significantly longer period of the AIRS data allows one to look into long-term changes in methane concentration and seasonal amplitude. We computed a pan-Arctic maps of seasonally resolved methane trends during last 17 years (Figure 3 for LT and Figure S6 for MT). Linear least squares regressions were calculated using MATLAB for each 1°x1° grid cell. This procedure allows us to locate regions with the highest growth rates. The lowest trends, between 2.5 and 3.5 ppb/year were found in summer over the mid-latitude Atlantic, Pacific, and some parts of the Arctic ocean including domain #3 (Figure 3b). Continental summer trends over were slightly higher: up to 4 ppb/year. The globally-averaged CH_4 trend for 2007–2014 was estimated from surface measurements as ~ 5–6 ppb/year (Saunois et al., 2020), though it increased after 2014 (Yurganov et al., 2017; Nisbet et al. 2019). A reduced sensitivity of the thermal IR remote technique to LT generally can lead to underestimation of methane changes (0.3-0.5, see Methods and Yurganov et al., 2016). This should be kept in mind while comparing LT satellite data with in situ surface measurements. On the other hand, sensitivity of the TIR technique to MT is higher and close to one. This is a reason for higher trends in MT (see Supplement Figure S6 and S7) . The maximal rate of long-

term winter LT methane growth up to 5.5 ppb/year was found to the north of the Kara Sea, as well as over the northern Sea of Okhotsk (Figure 3d) that was twice as large compared to the summer rate. From what was presented above, the central Barents Sea with the most strong water mixing might be expected to demonstrate the fastest winter growing. However, it was not the case: the largest winter trends were observed far to the North-East of that place, closer to the domain #2.

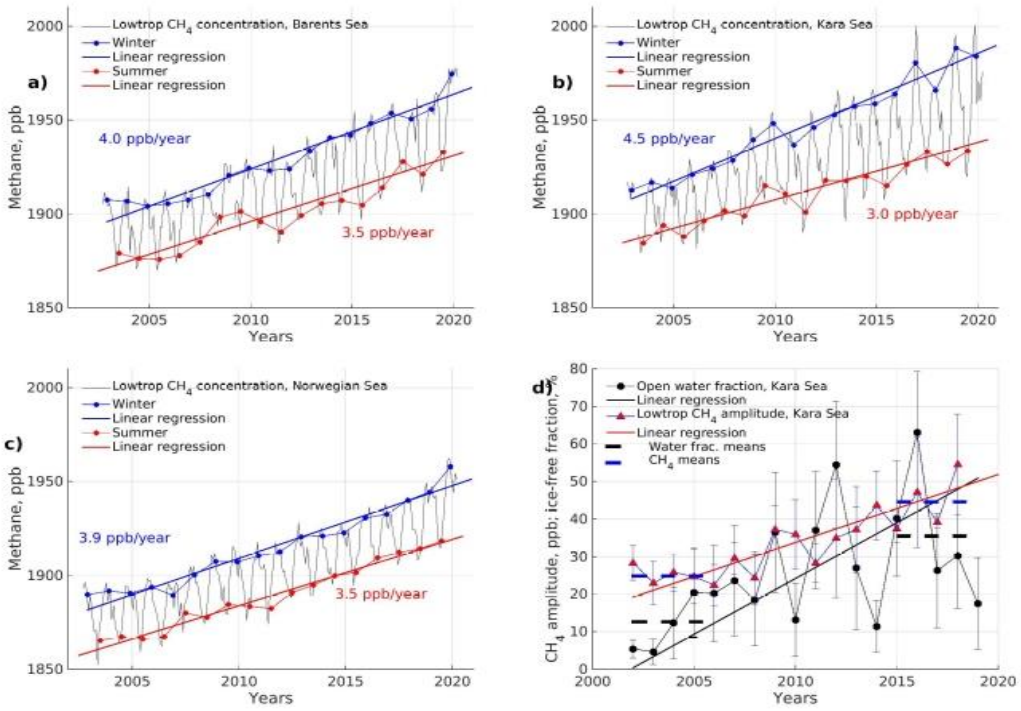

Figure 4

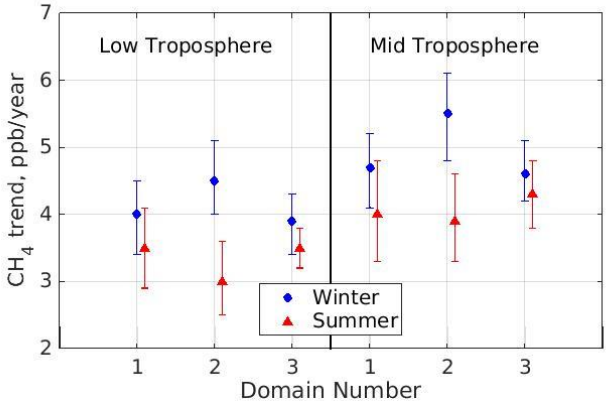

Figure 5

Figure 4 a, b, c show monthly mean methane concentrations for domains ## 1, 2, 3, respectively (thin black lines) and the amplitude trend for the domain #2 (winter minus summer, red), Figure 4d. Parameters of linear least square correlation are listed in Table and on a graph of Figure 5. For all domains winter trends are higher than summer trends, but the difference between them is statistically significant for domain #2 only. One may compare this trend with variations of the fraction of open water C_{wat}=100-C_{ice} , where C_{ice} is the fraction of ice in the same domain. Open water fraction really increased from 2002 to 2019, but huge year-to-year

variations impede a search of correlation.

Growing seasonal methane amplitude over of the Kara Sea domain needs to be explained at least in terms of secular changes in two transport mechanisms concerned in this paper. In spite of direct correlation between methane and water fraction, it is reasonable to compare the maps of open water and methane for the beginning and the end 5-year spans of data (spans are shown as dashed lines in Figure 4d). In a map of Figure 6a, the winter open-water fraction averaged over 2014–2018 was subtracted by that over 2002–2006. The northern BKS region has the fastest ice degradation in the Arctic Ocean (the indicated area between Svalbard, Severnaya Zemlya, and Kara Sea is called the "big polygon" henceforth). The Arctic-wide record fast decline in sea-ice in this area is a well known phenomenon that significantly disturbs the air circulation in Northern mid and high latitudes (Petoukhov and Semenov, 2010; Zhang et al, 2018b). Similarly, ice degradation during last 17 years may be a significant factor impacting the interannual variability of methane (Figure 6b). Correlation between them is poor: maximal increase of open water area is observed in the northernmost part of the big polygon, whereas CH_4 increased mostly close to NZ.

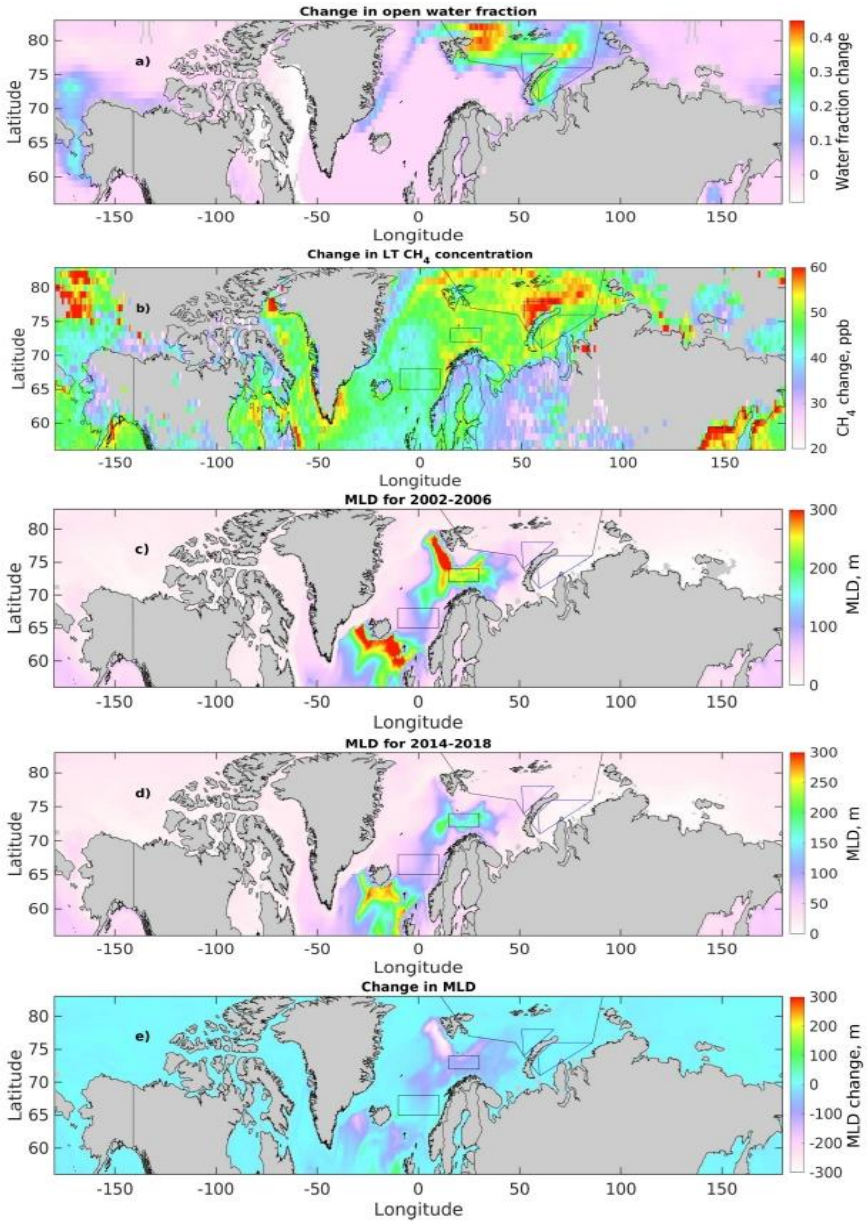

Figure 6

An illustration for that is Figure 7: methane for 1° × 1° pixels from Figure 6b was plotted versus corresponding pixels for open water fraction from Figure 6a. Methane for the big polygon and the Kara Sea polygon dramatically increases with increasing water fraction from 0.08 to 0.15, but plateaus after. The number of points for the NZ polygon for low water (high ice) conditions is insufficient to make any conclusions on connections with sea-ice cover decline there. Data presented in Figure 7 show that there may be several mechanisms causing methane increase in the big polygon since the beginning of this century, but growing area of open water is one of them.

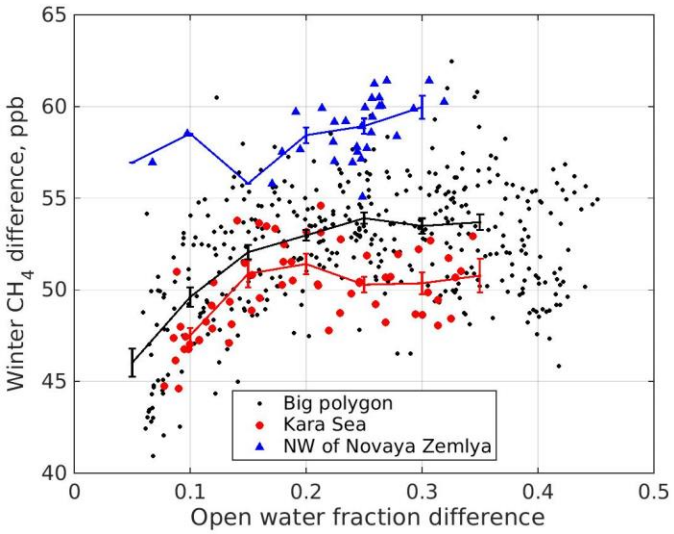

Figure 7

Long-term changes in MLD throughout the elapsed 17-year period may influence methane in BKS. To check a feasibility of this, winter MLD were averaged for the Arctic over the same 5-year spans and subtracted one from another (Figure 6 c,d, e). In contrast to C_{wat}, MLD diminished since the early 2000: changes were negative in the Barents Sea and west of Svalbard. This decrease may be connected with secular changes in seawater stability. The reasons for these require further analysis, but in fact this negative trend cannot be a reason for the observed methane positive trend.

4. Discussion

Seven currently operative TIR spectrometers launched at sun-synchronous polar orbits supply huge amounts of information about Arctic methane year-round, day and night. These TIR data are unique for studying CH_4 emissions from a warming Arctic, both terrestrial and marine. Results presented in this paper evidence in favor of wintertime Arctic seas as an important source area for the regional methane budget. In spite of a reduced sensitivity, preference has been made to methane in low troposphere. This atmospheric layer is supposed to be more closely linked with surface emissions. MT AIRS retrievals are more sensitive to CH_4 variations in this layer, but in the 4-6 km altitudes the long-range transfer of trace gases is very important. Nevertheless, MT data show patterns that similar to LT (Supplement Figures S6 - S8). Further investigation should be based on 3D modeling using actual wind fields.

Global methane emission is estimated by Saunois et al. (2020) as 576 Tg CH_4 per year. High latitude (60º N - 90º N) emission constitutes only 23 Tg CH_4 per year, i.e., ~4%. Marine emission is considered by Saunois et al. (2020) and Berchet et al. (2016) as negligible (<4 Tg CH_4 per year). Satellite data (Yurganov et al., 2016) are in agreement with low sea/air flux in summer, but in cold season the Arctic seas appear to contribute ~ 2/3 of annual continental emission (i.e., ~15 Tg CH_4 per year). In any case, even 38 Tg CH_4 per year is less than 7% of global budget. Growing amplitude of the CH_4 seasonal cycle, observed by AIRS over the Arctic shelf since 2003, evidence a growing winter flux. Nevertheless, the Arctic contribution hardly can be expected to surpass 10% of global emission even in the near future. Influence of growing CH_4 Arctic emission for the global trend should not be large. Contrary to that a regional influence may be significant. These speculations need a further investigation.

A thorough discussion of methane sources in the Arctic is beyond the scope of this study.

Our goal is just to indicate points of interest for further investigation. This study focuses at natural barriers for sea/ice exchange in BKS: summertime stable stratification and wintertime sea ice cover. In summer the pycnocline retains dissolved methane in deep layers and makes it available for methanotrophic bacteria. Atmospheric CH_4 concentration grows after November (Figure 2) concurrently with disappearance of the pycnocline and MLD deepening; its bottom boundary reaches a level of ~150 m. Available summer direct sounding data (Mau et al., 2017, Supplement Figure S9) indicate this depth as an upper boundary of high dissolved methane concentrations. Enhanced mixing facilitates gas transport to the surface and winter becomes a season of maximal methane flux to the atmosphere.

Second barrier is mostly important for seas that partially ice covered. Northern BKS ice cover has a distinct trend of degradation since the beginning of this century, especially in early winter (Figure 6a). Sea ice is a natural barrier for the flux and methane emission grows with years. Inter-relations between the flux and ice decay in winter may be more complicated. One can not exclude that the radiative forcing of excess methane may be a significant component in the warming of this area and, prospectively, for the whole Arctic. In other words, a positive feed-back is possible and investigation of methane emission from the Arctic seas must be intensified.

5. Conclusions

Data of three TIR orbital instruments for the Arctic seas allow to detect enhanced methane over BKS in winter. This finding highlights significant roles of turbulent diffusion in seawater depth and ice cover for the sea/air methane exchange. Enhanced mixing in winter resulted in a maximum of excess methane during that season in the western Barents Sea. 17-years long period of AIRS monitoring reveals an area with growing seasonal amplitude of both LT and MT methane: between Svalbard, Franz Josef Land, Novaya Zemlya and Severnaya Zemplya archipelagos. This is interpreted in terms of growing methane flux due to decay of ice cover: the area is known for record fast ice degradation. A trend in methane flux from the seabed itself was not considered here due to lacking experimental data.

Acknowledgments

We express our gratitude to personnel of NASA and NOAA that make publicly available satellite data on methane and sea ice concentration. Colm Sweeney (NOAA/GMD) kindly supplied data of aircraft sampling over the Trinidad Head, California.

Data availability statement. 1) AIRS/Aqua Level 3 monthly 1x1 lat/lon data are publicly available at the GES DISC, : https://disc.gsfc.nasa.gov/datasets/ (code of the data set AIRS3STM.006). 2) CrIS/SuomiNPP Level2 data are publicly available at GES DISC: https://disc.gsfc.nasa.gov/datasets/SNDRSNIML2CCPCCR_2/summary (code of the data set SNDRSNIML2CCPRET). 3) IASI-1/MetOp-A Level 2 data are publicly available at the https://www.avl.class.noaa.gov/saa/products/search?sub_id=0&datatype_family=IASI&submit.x=27&submit.y=10 archived by NOAA/CLASS. 4) Sea-ice concentration data are publicly available at the NASA National Snow and Ice Data Center Distributed Active Archive Center (https://nsidc.org/data/NSIDC-0081/versions/1). 5) MLD were computed using ECCO LLC270 global ocean and sea-ice data synthesis (Zhang et al., 2018a). 6) data of aircraft sampling are available upon request from Colm Sweeney (NOAA/GMD), Sweeney et al. (2016).

References

Årthun, M., Eldevik T. , and Smedsrud L. H. (2019), The role of Atlantic heat transport in future Arctic winter sea ice loss. *Journal of Climate, 32*, 3327–3341, https://doi.org/10.1175/JCLI-D-18-0750.1.

Berchet A., Bousquet P., Pison I., et al. (2016), Atmospheric constraints on the methane emissions from the East Siberian Shelf, *Atmospheric Chemistry and Physics*, *16*: 4147–

4157, https://doi.org/10.5194/acp-16-4147-2016.

Bloom H. J. (2001), The cross-track infrared sounder (CrIS): a sensor for operational meteorological remote sensing, in Fourier Transform Spectroscopy, *OSA Trends in Optics and Photonics*, *3*, 1341–1343, Optical Society of America , doi: 10.1109/IGARSS.2001.976838.

de Boyer Montégut D. Madec, G., Fischer, A. S., Lazar, A., and Iudicone, D. (2004), Mixed layer depth over the global ocean: An examination of profile data and a profile-based climatology, *Journal of Geophysical Research*, *109*, C12003, doi:10.1029/2004JC002378.

Cavalieri D. J., Parkinson C. L., Gloersen P., Zwally H. J. (1996), Sea Ice Concentrations from Nimbus-7 SMMR and DMSP SSM/I-SSMIS Passive Microwave Data, Version 1. Boulder, Colorado USA. NASA National Snow and Ice Data Center Distributed Active Archive Center, doi: https://doi.org/10.5067/8GQ8LZQVL0VL.

Comiso J. C., Parkinson C. L., Gersten R., Stock L(2008), Accelerated decline in the Arctic sea ice cover. *Geophysical Research Letters*,. *35*, L01703. doi: 10.1029/2007GL031972,

Fekete B. M., Vöröosmarty C. J., and Grabs W. (2002), High-resolution fields of global runoff combining observed river discharge and simulated water balances. *Global Biogeochemical Cycles*, *16*(3), 1042.

Fenty I., Menemenlis D., and Zhang H. (2017), Global Coupled Sea Ice-Ocean State Estimation. *Climate Dynamics*, *49*(3), 931–956.

Ferré B., Jansson P., Moser M., Serov P., Portnov A.D., Graves C. , Panieri G., Gründger F., Berndt C., Lehmann M.F., Niemann H. (2020), Reduced methane seepage from Arctic sediments during cold bottom-water conditions. *Nature Geoscience*, *13*, 144–148. https://doi.org/10.1038/s41561-019-0515-3

Forget, G., Campin, J.-M., Heimbach, P., Hill, C. N., Ponte, R. M., and Wunsch, C. (2015), ECCO version 4: an integrated framework for non-linear inverse modeling and global ocean state estimation. *Geoscientific Model Development*, *8*(10), 3071–3104.

Gambacorta, A. (2013), The NOAA unique CrIS/ATMS processing system (NUCAPS): algorithm theoretical basis documentation, available at: hhttp://www.ospo.noaa.gov/Products/atmosphere/soundings/nucaps/docs/NUCAPS_ATBD_20130821.pdf

Gent, P. and McWilliams J. (1990), Isopycnal mixing in ocean circulation models, *Journal of Physical Oceanography*, *20*, 150–155.

Gentz T., Damm E., von Deimling J. S., Mau S.,McGinnis D. F., Schlüter M. (2014), A water column study of methane around gas flares located at the West Spitsbergen continental margin. *Continental Shelf Research*, *72***,** 107- 118 . doi: 10.1016/j.csr.2013.07.013

Hoegh-Guldberg O. and Bruno J. F. (2010), The impact of climate change on the world's marine ecosystems. *Science*, *328*, 1523-1528. doi: 10.1126/science.1189930

James R. H., Bousquet P., Bussmann I., Haeckel M., Kipfer R., Leifer I., Niemann H., Ostrovsky I., Piskozub J., Rehder G., Treude T., Vielstadte L., Greinert J. (2016) Effects of climate change on methane emissions from seafloor sediments in the arctic ocean: a review. *Limnology and Oceanography*, *61***,** S283–S299. https://doi.org/10.1002/lno.10307

Kara, A. B., Rochford, P. A., & Hurlburt, H. E. (2000), An optimal definition for ocean mixed

layer depth. *Journal of Geophysical Research, 105*(C7), 16803–16821. doi:10.1029/2000JC900072.

Kara A. B., Rochford P. A., Hurlburt H. E. (2002), Mixed layer depth variability over the global Ocean. *Journal of Geophysical Research, 108*(C3), doi: 10.1029/2000JC000736

Maddy E. S., Barnet C. D., Gambacorta A. (2009), A computationally efficient retrieval algorithm for hyperspectral sounders incorporating a priori information. *IEEE Geoscience Remote Sensing Letters, 6,* 802–806, doi:10.1109/lgrs.2009.2025780.

Mau S., Romer M., Torres M.E., Bussmann I., Pape T., Damm E., Geprags P., Wintersteller P., Hsu C.W., Loher M., Bohrman G. (2017), Widespread Methane Seepage along the Continental Margin off Svalbard—From Bjornoya to Kongsfjorden. *Scientific Reports, 7,* 42997 https://doi.org/10.1038/srep42997

Menemenlis, D., Fukumori, I., & Lee, T. (2005a), Using Greens functions to calibrate an ocean general circulation model, *Monthly Weather Review, 133*, 1224–1240.

Menemenlis, D., Hill, C., Adcroft, A., Campin, J., Cheng, B., Ciotti, B., et al. (2005b). NASA supercomputer improves prospects for ocean climate research. *Eos Transactions AGU 86(9)*, 95–96. doi: 10.1029/2005EO090002

Menemenlis, D., Campin, J., Heimbach, P., Hill, C., Lee, T., Nguyen, A., Schodlock, M., & Zhang, H. (2008), ECCO2: high resolution global ocean and sea ice data synthesis, *Mercator Ocean Quarterly Newsletter, 31,* 13–21.

Myhre C.L., Ferré B., Platt S.M., Silyakova A., Hermansen O., Allen G., et al. (2016), Extensive release of methane from Arctic seabed west of Svalbard during summer 2014 does not influence the atmosphere, *Geophysical Research Letters, 43*, 4624–4631.

Myhre, G; Shindell, D.; Bréon, F.M.; Collins, W.; Fuglestvedt, J.; Huang, J.; Koch, D.; Lamarque, J.F.; Lee, D.; Mendoza, B.; Nakajima, T.; Robock, A.; Stephens, G.; Takemura, T.; Zhang, H. (2013), *Climate Change 2013: The Physical Science Basis. Contribution of Working Group I to the Fifth Assessment Report of the Intergovernmental Panel on Climate Change* , T. F. Stocker, D. Qin, G.-K. Plattner, M. Tignor, S.K. Allen, J. Boschung, A. Nauels, Y. Xia, V. Bex and P.M. Midgley, Cambridge University Press, Cambridge, United Kingdom and New York, NY, USA, 2013

Nisbet, EG; Manning, MR; Dlugokencky, EJ; Fisher, RE; Lowry, D; Michel, SE; Lund Myhre, C; Platt, SM; Allen, G; Bousquet, P; Brownlow, R; Cain, M; France, JL; Hermansen, O; Hossaini, R; Jones, Anna ; Levin, I; Manning, AC; Myhre, G; Pyle, JA; Vaughn, B; Warwick, NJ; White, JWC. (2019), Very strong atmospheric methane growth in the four years 2014 - 2017: Implications for the Paris Agreement. *Global Biogeochemical Cycles*, *33*(3). 318-342. https://doi.org/10.1029/2018GB006009

Olivier, J.G.J., Van Aardenne, J.A., Dentener, F., Pagliari, V., Ganzeveld, L.N., & Peters, J.A. (2005), Recent trends in global greenhouse gas emissions: regional trends 1970-2000 and spatial distribution of key sources in 2000. *Environmental Sciences, 2* (2-3), 81-99. doi: 10.1080/15693430500400345.

Petoukhov V., Semenov V. A. (2010), A link between reduced Barents Kara sea ice and cold winter extremes over northern continents. *Journal of Geophysical Research, 115*, D21111. doi:10.1029/2009JD013568.

Portnov A., Mienert J., Serov P. (2014), Modeling the evolution of climate sensitive Arctic subsea permafrost in regions of extensive gas expulsion at the West Yamal shelf. *Journal*

of Geophysical Research: *Biogeosciences*, *119*(11): 2082-94. https://doi.org/10.1002/2014JG002685

Razavi A., Clerbaux C., Wespes C., Clarisse L., Hurtmans D., Payan S., Camy-Peyret C., & Coheur P. (2009), Characterization of methane retrievals from the IASI space-borne sounder. *Atmospheric Chemistry and Physics*, *9*, 7889-7899.

Redi, M. H. (1982), Oceanic isopycnal mixing by coordinate rotation. *Journal of Physical Oceanography*, *12*, 1154–1158.

Rudels, B. (1993), High latitude ocean convection. In Flow and Creep in the Solar System: Observations, Modelling and Theory, pp. 323–356. Ed. by D. B. Stone and S. K. Runcorn. Academic Publishers, Dordrecht.

Saunois M. et al. (2020), The global methane budget 2000–2020. *Earth System Scientific Data*, *12*, 1561–1623, https://doi.org/10.5194/essd-12-1561-2020.

Serov, P., Vadakkepuliyambatta, S., Mienert, J., Patton, H., Portnov, A., Silyakova, A., et al. (2017), Postglacial response of Arctic Ocean gas hydrates to climatic amelioration. *Proceedings of the National Academy of Sciences* , *114*(24), 6215–6220. doi:10.1073/pnas.1619288114

Shipilov E. V., Murzin R. R. (2002), Hydrocarbon deposits of western part of Russian shelf of Arctic—Geology and systematic variations. *Petroleum Geology*, *36*(4): 325–347. [Translated from Geologiya Nefti i Gaza. 2001, no. 4, 6–19.]

Skagseth, Ø., Eldevik, T., Årthun, M. et al. Reduced efficiency of the Barents Sea cooling machine. *Nature Climatic Change*, *10*, 661–666 (2020). https://doi.org/10.1038/s41558

Smith, N., and Barnet C. D. (2019), Uncertainty characterization and propagation in the Community Long-term Infrared Microwave Combined Atmospheric Product System (CLIMCAPS). *Remote Sensing*, *11*, 1227, https://doi.org/10.3390/rs11101227.

Suga, T., K. Motoki, Y. Aoki, and A. M. Macdonald (2004), The North Pacific climatology of winter mixed layer and mode waters. *Journal of Physical Oceanography*, *34*, 3–22.

Susskind, J., Blaisdell J. M., and Iredell L. (2014), Improved methodology for surface and atmospheric soundings, error estimates, and quality control procedures: The Atmospheric Infrared Sounder science team version-6 retrieval algorithm. *Journal of Applied Remote Sensing*, *8*(1), 084994, https://doi.org/10.1117/1.JRS.8.084994.

Sweeney, C., Dlugokencky, E., Miller, C. E., Wofsy, S., Karion, A., Dinardo, et al. (2016), No significant increase in long-term CH_4 emissions on North Slope of Alaska despite significant increase in air temperature. *Geophysical Research Letters*, *43*, 6604–6611, doi:10.1002/2016GL069292

Wunsch, C., Heimbach, P. Ponte, R., and Fukumori, I. (2009), The global general circulation of the ocean estimated by the ECCO-consortium. *Oceanography, 22*, 88-103.

Xiong X, Barnet C, Maddy E, Sweeney C., Liu X., Zhou L., Goldberg M. (2008), Characterization and validation of methane products from the Atmospheric Infrared Sounder (AIRS). *Journal of Geophysical Research* , *113***,** G00A01, doi:10.1029/2007JG000500.

Xiong X., Barnet C., Maddy E., Gambacorta A., King T., and Wofsy S. (2013), Mid-upper tropospheric methane retrieval from IASI and its validation, *Atmospheric Measurement Techniques*, *6*, 2255-2265.

Yurganov L. N., Leifer I., Myhre C. L. (2016), Seasonal and interannual variability of atmospheric methane over Arctic Ocean from satellite data. *Sovremennye problemy distantsionnogo zondirovaniya zemli iz kosmosa (Current Problems of Remote Sensing of Earth From Space), 13*(2): 107-119, doi:10.21046/2070-7401-2016-13-2-107-119

Yurganov L.N., Leifer I., and Vadakkepuliyambatta, S. (2017), Evidences of accelerating the increase in the concentration of methane in the atmosphere after 2014: satellite data for the Arctic), *Sovremennye problemy distantsionnogo zondirovaniya zemli iz kosmosa (Current Problems of Remote Sensing of Earth From Space), 14(5)*, 248-258. doi: 10.13140/RG.2.2.16613.29927

Yurganov L., Muller-Karger F., Leifer I. (2019), Methane increase over the Barents and Kara Seas after the autumn pycnocline breakdown: Satellite observations. *Advances in Polar Science*, *30*(4):382-390. doi: 10.13679/j.advps.2019.0024

Zhang, H., Menemenlis, D., and Fenty, I. G. (2018a), ECCO LLC270 Ocean-Ice State Estimate, https://doi.org/1721.1/119821

Zhang Q., Xiao C., Ding M., Dou T. (2018b), Reconstruction of autumn sea ice extent changes since AD1289 in the Barents-Kara Sea, Arctic. *Science China Earth Science*, *61*, 1279–1291. https://doi.org/10.1007/s11430-017-9196-4

Figure captions.

Figure 1. Methane concentrations retrieved from AIRS TIR radiance data for the layer 0-4 km (LT) for 4 seasons: spring (a), summer (b), autumn (c), winter (d) between February, 2019 an January, 2020. Blank areas correspond to insufficient vertical air temperature contrast (ThC<10° C). See also the same for MT (Supplement, Figure S5).

Figure 2. LT (0-4 km altitude) CH_4 anomaly, i.e. a concentration difference between the Barents Sea domain #1 and Norwegian Sea domain #3 (see map Figure 1). IASI and AIRS data are averaged over 2010-2018, CrIS data are for 2015-2018. Blue lines are 2010-2018 averaged MLD for the Western Barents Sea domain #1 (see map) for 3 criteria (#1 is by Suga et al. (2004), #2 is Kara et al. (2000) , #3 is Boyer et al. (2004).

Figure 3. Maps of LT methane trends derived from 2002-2019 data of AIRS. Slopes of standard linear regression lines for 4 seasons: spring (a), summer (b), autumn (c), winter (d) were computed for each 1°x1° lat/lon pixel. Blank areas correspond to insufficient vertical air temperature contrast (ThC<10° C) . See also the same for MT (Supplement, Figure S6).

Figure 4. Methane LT concentrations and trends according to AIRS data. Monthly mean methane concentrations are averaged for domains, designated on the maps of Figure 1: a) #1, b) #2, and c) #3. Regression lines are plotted for winter and summer periods, slopes are shown (see also Table and Figure 5). d): Amplitudes of seasonal cycles for Kara Sea domain #2 are computed as difference between CH_4 for winter period and for the next summer period. They are compared with mean fractions of open water for the same domain in winter (November-January). Dash lines are CH_4 and C_{wat} averaged for the first and last 5-year spans. See also the same for MT (Supplement, Figure S7).

Figure 5. Slopes of regression lines for two seasons, three domains, and two altitude ranges. Error bars correspond to Lower and Upper bounds of confidence intervals for slope (reliability 95%). See also Table.

Figure 6. Maps of open water fraction, CH_4 and MLD (criterion #2). a) Changes in winter open water fraction averaged over the first 2002-2006 and last 2014-2018 spans of AIRS measurement period. b) The same, but for LT CH_4 concentration. c) MLD for 2002-2006. c) MLD for 2014-2018. e) Map d) subtracted by map c).

Figure 7. Spacial correlation between changes in open water fraction (Fig. 6a) and LT methane concentrations (Fig. 6b) for big polygon and two sub-polygons (indicated on the maps of Figures 6a and 6b). Each point corresponds to 1°x1° pixel. Lines connect averages for binned CH_4, error bars are $STD \cdot N^{-1/2}$, where STD are standard deviations for binned data, N is number of points.

Table

Linear Regression Parameters For CH_4 Seasonal Means in ppb/year. LBCI Is Lower Bound of Confidence Interval for Slope; UBCI is Upper Bound of Confidence Interval for Slope (reliability 95%). See also Figure S8. R is correlation coefficient

Domain	**Layer**	**Season**	**Slope**	**LBCI**	**UBCI**	**R**
1	LT	Winter	4.0	3.4	4.5	0.94
2	LT	Winter	4.5	4.0	5.1	0.95
3	LT	Winter	3.9	3.4	4.3	0.95
1	MT	Winter	4.7	4.1	5.2	0.94
2	MT	Winter	5.5	4.8	6.1	0.95
3	MT	Winter	4.6	4.2	5.1	0.96
1	LT	Summer	3.5	2.9	4.1	0.90
2	LT	Summer	3.0	2.5	3.6	0.89
3	LT	Summer	3.5	3.2	3.8	0.97
1	MT	Summer	4.0	3.3	4.8	0.88
2	MT	Summer	3.9	3.3	4.6	0.90
3	MT	Summer	4.3	3.8	4.8	0.96
1	LT	Win.-Summ.	1.3	0.7	1.9	0.34
2	LT	Win.-Summ.	2.2	1.4	3.0	0.55
3	LT	Win.-Summ.	0.9	0.5	1.3	0.25
1	MT	Win.-Summ.	1.6	0.9	2.3	0.38
2	MT	Win.-Summ.	2.5	1.5	3.4	0.52
3	MT	Win.-Summ.	1.0	0.6	1.5	0.28